



# Shear band stability and uniform elongation of gradient structured material: Role of lateral constraint

Yanfei Wang<sup>a</sup>, Chongxiang Huang<sup>a,\*</sup>, Zhongkai Li<sup>b</sup>, Xiaotian Fang<sup>b</sup>, Mingsai Wang<sup>a</sup>, Qiong He<sup>a</sup>, Fengjiao Guo<sup>a</sup>, Yuntian Zhu<sup>b,c,\*\*</sup>

<sup>a</sup> School of Aeronautics and Astronautics, Sichuan University, Chengdu 610065, China

<sup>b</sup> Department of Materials Science and Engineering, North Carolina State University, Raleigh, NC 27695, USA

<sup>c</sup> Nano and Heterogeneous Structural Materials Center, School of Materials Science and Engineering, Nanjing University of Science and Technology, Nanjing 210094, China

## ARTICLE INFO

### Article history:

Received 22 October 2019

Received in revised form 17 March 2020

Accepted 17 March 2020

Available online 8 April 2020

### Keywords:

Gradient structure

Shear bands

Uniform elongation

Synergistic constraint

Heterostructure

## ABSTRACT

Here we report a shear bands-dominated deformation principle for the gradient material composed of two nanostructured gradient layers (NGLs) and a coarse-grained (CG) interior. Multiple shear bands form in the NGL to accommodate the applied strain. The magnitude of uniform elongation depends on shear band stability, and shear band stability is determined by the intensity of constraint between NGL and CG interior. Specifically, the stronger the constraint, the denser and more stable the shear bands dispersed in the NGL, thereby leading to larger uniform elongation. This finding sheds insight into the theoretical basis of harnessing dispersed stable shear bands in heterostructures by optimizing microstructure architecture.

© 2020 Elsevier Ltd. All rights reserved.

## 1. Introduction

As one of the heterostructures, the gradient structure with a systematic change in microstructure from nanostructured (NS) surface to coarse-grained (CG) interior has attracted extensive interests for its potential in alleviating strength–ductility trade-off [1–4]. For example, a combination of several times higher yield strength and decent uniform elongation (compared with that of the homogeneous CG counterpart) was achieved in gradient Cu [5,6], IF steel [7,8] and multiphase steels [9–11]. Recent investigations found that the heterogeneous deformation of component layers can significantly promote the development of long-range internal stresses, leading to extra strength and work hardening [7,12–15], i.e., hetero-deformation induced strengthening and hardening [16]. These explained the origin of high strength. However, physics behind the large uniform elongation of gradient structure are not thoroughly understood, especially in the NS surface layer, which is believed to have intrinsically low ductility when it is tensile deformed alone.

Uniform elongation of metals is generally evaluated as the strain before the formation of catastrophic strain localization

under uniaxial tension [17]. Since the NS surface layer is difficult to accommodate large plastic strain via homogeneous (on macro-scale) activity of crystalline defects as normally observed in CG materials, there is a high possibility that the applied tensile strain is largely accommodated by some type of non-localized strain concentrations. Delocalized propagation of individual strain concentration zones along gauge length was observed in the NS layer of gradient IF steel [18]. This deformation mode is new but seems not universal for most gradient structures. Recent investigations in the straining behavior of ultrafine-grain/CG, NS/CG and NS/ductile dendrite heterostructures indicated that microstructure heterogeneity could promote the nucleation of shear bands (SBs) from domain boundaries/interfaces due to stress concentration [19–21]. This inspired us to check the role of SBs in the deformation of gradient material. Surprisingly, dense SBs were indeed detected in the NS surface layer of gradient Ni [22]. These SBs evolved to accommodate a large strain without instability. However, reasons for the stable evolution and the factors controlling the stability still remain unclear. These are critical to understanding the deformation and failure fundamentals of gradient structured materials.

To study the above issue, the plastic behaviors of a series of gradient Ni specimens, with same microstructure gradient but varying gauge width, are characterized using digital image correlation. It is found that the uniform elongation is significantly reduced as the SBs become unstable, and the stability of SBs depends on the constraint from CG layer.

\* Corresponding author.

\*\* Corresponding author at: Department of Materials Science and Engineering, North Carolina State University, Raleigh, NC 27695, USA.

E-mail addresses: [chxhuang@scu.edu.cn](mailto:chxhuang@scu.edu.cn) (C. Huang), [ytzhu@ncsu.edu](mailto:ytzhu@ncsu.edu) (Y. Zhu).

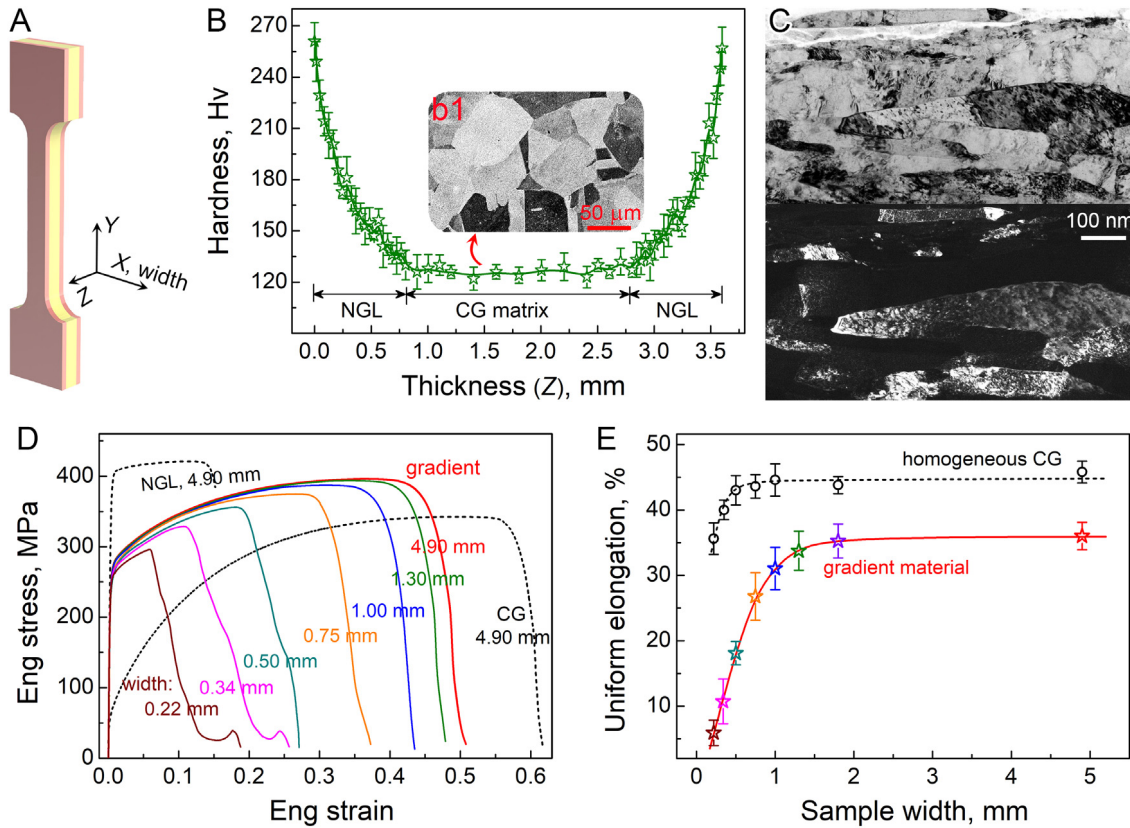


**Fig. 1.** (A) Geometry of tensile specimen cut from gradient plate. In the coordinate,  $Y$  and  $X$  represent the tensile loading direction and the specimen width direction, respectively.  $Z$  is the specimen thickness direction with mechanical/microstructural gradient. (B) Micro-hardness profile measured along the thickness of gradient material. Inset (b1) is an electron micrograph showing the CG center of gradient material. (C) Bright and dark field TEM images taken from the topmost NS layer. (D) Tensile responses of gradient specimens with varying width (colored solid curves), freestanding NGL and homogeneous CG (black dotted curves). The number near each curve represents the width of tensile specimen. (E) Uniform elongation of gradient (colored data) and homogeneous CG (black data) specimens with varying width.. (For interpretation of the references to color in this figure legend, the reader is referred to the web version of this article.)

## 2. Experiments

Gradient Ni material was symmetrically processed by rotationally accelerated shot peening on both sides of an annealed plate with a thickness of 3.6 mm [23]. The peening process on each side was firstly conducted using 1-mm-diameter steel balls at a velocity of 40 m/s for 5 min, and then treated using smaller balls (0.5 mm in diameter) to reduce surface roughness. Microstructure of gradient material was characterized using transmission electron microscopy (TEM, FEI Tecnai G2 T20). Focused ion beam was used to extract TEM foils.

As the dog-bone shaped geometry illustrated in Fig. 1A, gradient tensile specimens with a constant gauge length (18 mm) but varying width (4.90 mm–0.34 mm) were machined from the as-processed gradient plate. The shoulder width of tensile specimens was 4.3 mm. Tensile tests for each type of specimen were repeated at least three times at a constant strain rate of  $5 \times 10^{-4} \text{ s}^{-1}$ , and an extensometer was used to measure the tensile strain. Speckle images on specimen surface were recorded *in-situ* using a short-focus optical lens (9.7  $\mu\text{m}/\text{pixel}$  in resolution) for strain calculation [22]. The distribution of Vickers hardness along the thickness was measured at a load of 25 g for 15 s.

## 3. Results and discussion

The microhardness decreased gradually from  $\sim 260$  Hv in the topmost surface to  $\sim 127$  Hv in the central matrix (Fig. 1B), resulting in large mechanical gradient in the top  $\sim 760 \mu\text{m}$ -thick layer. The gradual change of hardness indicates a continuous

transition of microstructure. Inset in Fig. 1B shows the equiaxial CG microstructure in the central matrix. Fig. 1C presents typical bright and dark field TEM micrographs taken from the topmost surface layer. Obviously, this layer is composed of largely elongated nanostructures with high dislocation density and individual well-developed nanograins.

For comparison, tensile specimens containing only the top 760  $\mu\text{m}$ -thick layer or the central 2.0-mm-thick core were prepared by polishing away the other layers, and referred to as freestanding nanostructured gradient layer (NGL) and homogeneous CG matrix, respectively. The engineering tensile stress-strain responses of gradient specimens (colorful solid curves), freestanding NGL and CG matrix (black dotted curves) are compared in Fig. 1D. As shown, the freestanding NGL displays much higher yield strength but lower uniform elongation as compared to CG matrix, indicating significant mechanical incompatibilities in the elastic limit, uniform elongation and strain hardening capability between them. The gradient specimen with large width (4.90 mm, the red solid curve) exhibits an excellent combination of uniform elongation and strength, a uniform elongation of  $\sim 80\%$  of that in homogeneous CG material and simultaneously a yield strength that is  $\sim 4$  times as high.

Interestingly, a dramatic decrease in uniform elongation occurred for gradient specimens when the width is smaller than 1.5 mm (Fig. 1D). As the variation of uniform elongation summarized in Fig. 1E and Table 1, it is decreased to even less than 10% as the specimen width is smaller than 0.3 mm. Note that this unique effect induced by specimen dimension is more serious than the size effect in conventional homogeneous materials that

**Table 1**

The uniform elongation and corresponding deviation limit of gradient and homogeneous CG materials with varying specimen width. The deviation limit was obtained from the tests of at least three independent specimens.

Specimen width (mm)		4.90	1.80	1.30	1.00	0.75	0.50	0.34	0.22
Gradient	Average	35.8%	35.2%	33.7%	31.0%	26.7%	18.1%	10.7%	5.9%
	Deviation limit	±2.1%	±2.6%	±2.8%	±3.2%	±3.6%	±1.8%	±3.4%	±1.9%
Homogeneous CG	Average	45.2%	43.8%	–	44.6%	43.6%	43.0%	39.7%	35.6%
	Deviation limit	±1.6%	±1.3%	–	±2.5%	±1.7%	±2.2%	±1.5%	±2.4%

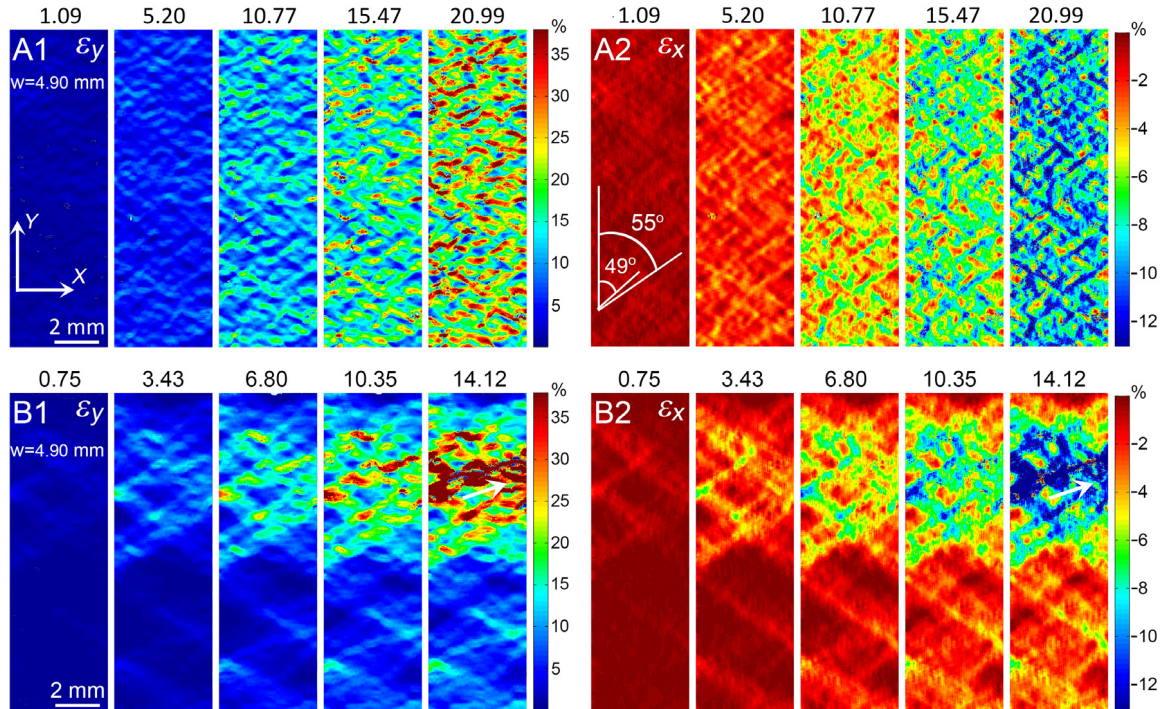


**Fig. 2.** Distribution of strains  $\varepsilon_y$  (the left column) and  $\varepsilon_x$  (the right column) measured on the NS surface ( $XOY$  plane) of gradient specimen [22] (A1–A2) and freestanding NGL (B1–B2), showing the evolvement of SBs with increasing applied strain.  $w$  represents specimen width. The number above each subgraph represents applied tensile strain. Shear bands are warm-colored in  $\varepsilon_y$  contour and cold-colored in  $\varepsilon_x$  contour.

was governed by the competition of dislocation activities in the surface grains and interior grains [24]. For example, the critical dimension controlling the start of size effect in homogeneous NS is generally smaller than the smallest width of present gradient specimens, i.e.,  $\sim 0.2$  mm [25]. The uniform elongations of homogeneous CG specimens cut from as-annealed plate with the same dimensions of gradient specimens were also examined. As shown (see the black data in Fig. 1E and the detailed value in Table 1), the drop of uniform elongation is started at a critical width of  $\sim 0.4$  mm, and it is only decreased by  $\sim 9.6\%$  as the width reduced to 0.22 mm. These observations suggest that the uniform elongation of gradient structures is dominated by some type of unusual plastic mechanism that is different from that in homogeneous NS and CG counterparts.

The distribution and evolution of strains measured on the NS surface of gradient specimen and freestanding NGL (4.90 mm in widths) are compared in Fig. 2. Dense macroscopic SBs were uniformly dispersed over the whole NS surfaces of gradient specimen (Figs. 2A1 and A2), which carried relatively high strain but none of them evolved to serious strain concentration to dominant fracture. In other words, these SBs were stable during tension and evenly accommodated the majority of applied strain. In contrast, in the freestanding NGL without CG matrix the coalescence of catastrophic shear localization was quickly developed at an early strain stage (Figs. 2B1 and B2), and there was only individual large SBs in the uniform gauge section. These observations clarify two critical points: (i) the excellent uniform elongation of gradient

structure and its NS surface layer (Fig. 1D) is accommodated by dispersed SBs; (ii) the stability of SBs in NS surface layer largely depends on the constraint from CG matrix.

The formation of dispersed shear bands in gradient structure can be primarily attributed to the low strain hardening capability of NS surface layer and the constraint from CG matrix [19, 22]. Under tension, stress concentration readily occurs in the NS surface layer soon after yielding due to the limited strain hardening rate and the triaxial internal stresses caused by elastic-plastic incompatibility, which will promote local shear instability, i.e., formation of early SBs [8, 26]. However, as discussed later, such local instability can be effectively constrained and passivated by the stable CG interior, which has higher strain hardening efficiency, thereby cannot quickly propagate across the whole cross-section as that usually observed in freestanding NGL [7, 19, 21]. The suppressed early SBs thus cannot release the stress concentration in the regions away from them, which permits the multiplication of more SBs until they are dispersed over the whole NS layer [27, 28].

To probe the underlying mechanism behind the specimen width-dominated variation of uniform elongation, we examined the propagation of SBs along the thickness direction by characterizing the strain evolution on the lateral surface (the  $YOZ$  plane illustrated in Fig. 1A) of gradient specimens. Surprisingly, with the change of specimen width SBs exhibit obviously different morphology and propagation rate (Fig. 3).

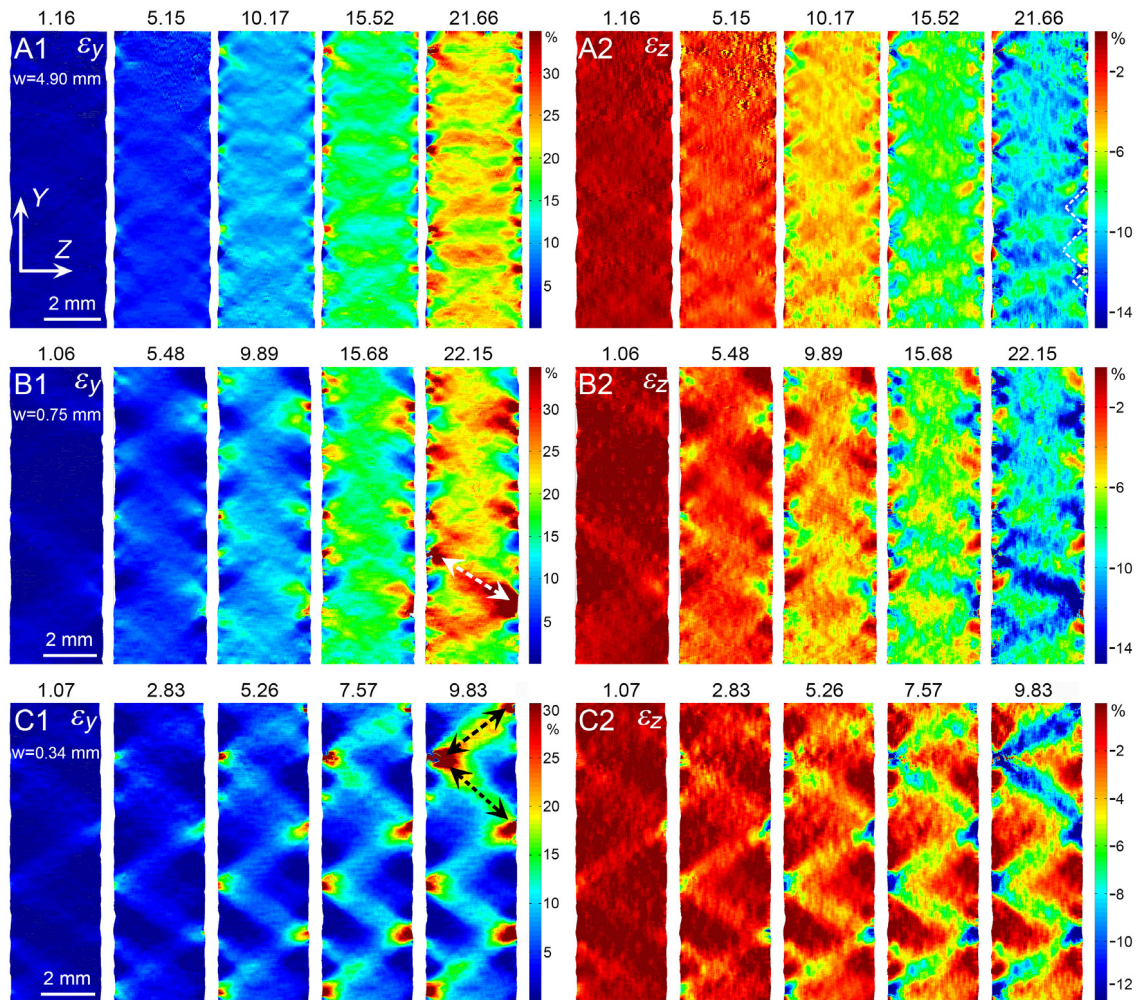


**Fig. 3.** SB morphology and evolution characterized on the lateral surface ( $YOZ$  plane) of gradient specimens in width of (A1–A2) 4.90 mm, (B1–B2) 0.75 mm, and (C1–C2) 0.34 mm. The left column is  $\varepsilon_y$  contour, and the right column is  $\varepsilon_z$  contour. Shear bands are cold-colored in  $\varepsilon_z$  contour. Dotted white lines in the last subgraph of (A2) mark the intersection of stable SBs. Double-angled lines in (B1) and (C1) indicate the formation of catastrophic shear bands.

For the wide specimen (Figs. 3A1 and A2), dense SBs nucleated from NS surface and then propagate along the thickness with a significant reduction in strain intensity. They intersected each other at a depth of  $\sim 600 \mu\text{m}$  and remained arrested by CG interior during the entire tension. In contrast, SB density was significantly reduced with decreasing specimen width, and individual SBs readily penetrated to the CG interior to connect with the band emitted from opposite side, as indicated by double-angled lines in Fig. 3B1 and C1. Taking the 0.34-mm-wide specimen as an example (Figs. 3C1 and C2), five stout SBs even quickly penetrated through the thickness to form a zigzag morphology before a global tensile strain of 3%, although the strain concentration in them was not extremely serious to cause immediate fracture. The SBs density, i.e., the average total number of SBs per unit gauge length, for specimens with varying width was statistically calculated from these strain maps. As shown in Fig. 4, the uniform elongation decreases almost linearly with SBs density as the specimen width becomes small. These results demonstrate that (i) the drop of uniform elongation with decreasing specimen width is due to the reduced SB density and stability, and (ii) the arrest/constraint efficiency of CG matrix on SBs propagation largely depends on specimen width.

The arrest of SBs propagation by the CG matrix was realized by the mutual constraint with NGL [7,29]. Since all gradient specimens have exactly the same microstructure gradient and there is no heterogeneity in width direction, it is interesting to find how

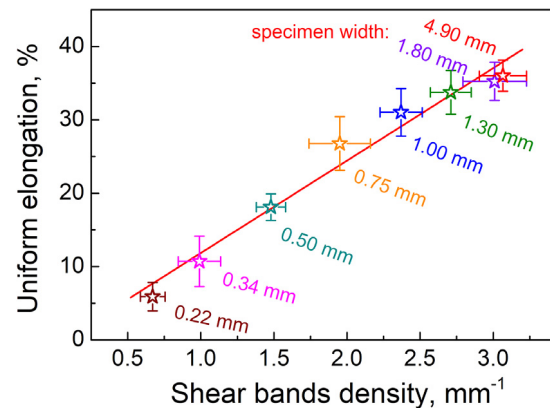


**Fig. 4.** SBs density vs. uniform elongation. The SBs density was statistically calculated from the strain maps in Fig. 3.

the specimen width affects the mutual constraint between CG matrix and NGL. To reveal the physics behind this, we analyzed the constraint stress state in gradient specimens with varying width by means of the finite element method (FEM, ABAQUS 6.14 package).

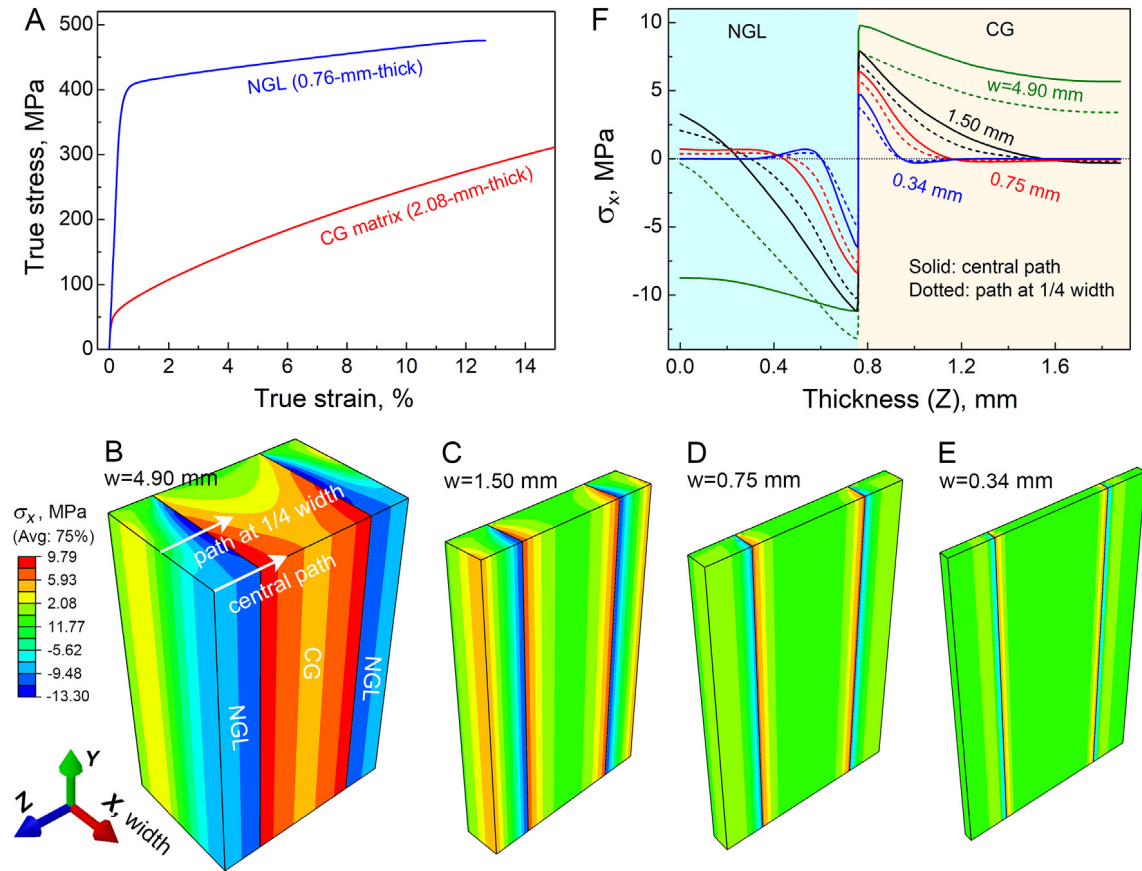


**Fig. 5.** FEM modeling of the variation of mutual constraint between NGL and CG layers with decreasing specimen width. (A) Stress–strain properties used for the NGL and CG parts in FEM. (B–E) Contours of the lateral constraint stress  $\sigma_x$  in the  $1/4$  model of gradient specimens in widths ( $w$ ) of 4.90 mm, 1.5 mm, 0.75 mm and 0.34 mm, at a tensile strain of 0.4%. White arrows in (B) mark the central path and the path at  $1/4$  width. (F) Comparison of the linear distribution of the constraint stress  $\sigma_x$ .

Since both gradient and laminate structures share the same deformation mechanisms in mechanical incompatibility-induced mutual constraint between layers, gradient structure can be approximately regarded as a special heterostructured laminate with multiple interfaces [8]. To simplify the analysis model and qualitatively assess the intensity of constraint between CG matrix and NGL, we consider the NGL as an isotropic homogeneous layer and simplify the gradient sample as a laminate with a CG core sandwiched by two NGLs. The true stress–strain responses under uniaxial tension (Fig. 5A) are used as the constitutive property of model parts.

Figs. 5B–F present the analysis results at a uniaxial tensile strain of 0.4%, i.e., a strain stage soon after yielding. As shown in Figs. 5B–E, componential layers are subjected to extra normal stresses in the width direction  $X$ ,  $\sigma_x$ .  $\sigma_x$  is negative in the NGL, but positive in the CG core, indicating that the NGL is subjected to a lateral compressive constraint from CG core at this strain stage. This mutual constraint is caused by the incompatibility of lateral shrinking strain  $\varepsilon_x$  that induced by the difference in elastic limit between layers [8,30]. Interestingly, for the models with varying width, both the magnitude and distribution of  $\sigma_x$  along thickness are obviously different. Fig. 5F plots the linear distribution of  $\sigma_x$  across the interface between NGL and CG core. As comparison,  $\sigma_x$  is lower and its distribution region across interface is thinner as the sample gets narrower. For example,  $\sigma_x$  in 4.90-mm-wide sample is much higher and distributed over much thicker region than that in the narrow samples (0.75 mm and 0.34 mm in widths). Note that there is no other significant normal or shear constraint between layers. These results suggest that reducing

the width of gradient specimen can lead to weaker constraint intensity and thinner constraint zone.

It was revealed that the fast multiplication of SBs in NGL is at the low-strain stage soon after yielding [22]. At this stage, the compressive constraint from CG interior plays a role in increasing the propagation resistance of SBs in NGL by closing and shielding the SB tip. This effect is similar to the impeding effect of ductile reinforcements on propagating plastic damages [21,31]. In addition, the extra stress  $\sigma_x$  makes the applied uniaxial stress to a multiaxial state, which promotes the strain hardening of NGL layer by activating more slip systems [7,32], thereby helping with stabilizing the propagating SBs. These stabilization effects on SBs propagation should be not significant if the constraint stress  $\sigma_x$  is weak. This is the reason why SBs in the narrower specimen with weaker constraint intensity exhibit lower stability (Fig. 3). The global stress will be released if the early SBs penetrate through whole cross-section, which obliterates the opportunity to nucleate new SBs in the less optimal regions. This is the primary reason for the low SB density (Figs. 3 and 4) and the slightly reduced flow stress (Fig. 1D) in narrow specimens.

The SB stability may be also affected by the mechanical gradient, the volume fraction of component layers and the materials properties such as stacking fault energy, which implies that the critical width at which uniform elongation begins to drop may be varied depending on the detailed microstructure gradient and material. This demands more experimental and theoretical explorations. It was suggested that nucleating multiple SBs in the harder domain (with low strain hardening efficiency) might be a universal plastic response for the hetero-deformation induced

high internal stress in heterostructures [16,19,33]. Although for the heterostructures with different microstructure architecture the SBs morphologies are different, the fundamental in all of them should be that the stronger the constraint between domains, the more stable the SBs and the larger uniform elongation can be achieved.

#### 4. Conclusion

In summary, our observations revealed that SBs play a dominant role in the uniform elongation of gradient structure. The uniform elongation is determined by SB stability, and SB stability depends on the mutual constraint between NGL and CG matrix. Specifically, in the wide specimen strong constraint led to the formation of dense dispersed SBs in the NGL, which remained stable during the entire tension and thus resulted in a superior uniform elongation comparable to that of homogeneous CG. SB stability was significantly reduced as the constraint became weaker with decreasing specimen width. Such unstable SBs quickly penetrated through the cross-section, leading to early fracture and limited uniform elongation. These findings demonstrate that SBs can be stabilized to improve the uniform elongation of NS materials by designing optimal heterogeneous architecture with strong constraint between component domains.

#### Declaration of competing interest

The authors declare that they have no known competing financial interests or personal relationships that could have appeared to influence the work reported in this paper.

#### Acknowledgments

This work was supported by the National Key R&D Program of China (2017YFA0204403), the National Natural Science Foundation of China (Nos. 11672195, 51931003) and Sichuan Youth Science and Technology Foundation (2016JQ0047). Y.T.Z. was funded by the US Army Research Office.

#### References

- [1] X.L. Wu, Y.T. Zhu, Heterogeneous materials: a new class of materials with unprecedented mechanical properties, *Mater. Res. Lett.* 5 (2017) 527–532, <http://dx.doi.org/10.1080/21663831.2017.1343208>.
- [2] E. Ma, T. Zhu, Towards strength–ductility synergy through the design of heterogeneous nanostructures in metals, *Mater. Today* 20 (2017) 323–331, <http://dx.doi.org/10.1016/j.mattod.2017.02.003>.
- [3] K. Lu, Making strong nanomaterials ductile with gradients, *Science* 345 (2014) 1455–1456.
- [4] I.A. Ovid'ko, R.Z. Valiev, Y.T. Zhu, Review on superior strength and enhanced ductility of metallic nanomaterials, *Prog. Mater. Sci.* 94 (2018) 462–540, <http://dx.doi.org/10.1016/j.pmatsci.2018.02.002>.
- [5] T.H. Fang, W.L. Li, N.R. Tao, K. Lu, Revealing extraordinary intrinsic tensile plasticity in gradient nano-grained copper, *Science* 331 (2011) 1587–1590, <http://dx.doi.org/10.1126/science.1200177>.
- [6] Y.F. Wang, F.J. Guo, Q. He, L.Y. Song, M.S. Wang, A.H. Huang, Y.S. Li, C.X. Huang, Synergetic deformation-induced extraordinary softening and hardening in gradient copper, *Mater. Sci. Eng. A* 752 (2019) 217–222, <http://dx.doi.org/10.1016/j.msea.2019.03.020>.
- [7] X.L. Wu, P. Jiang, L. Chen, F.P. Yuan, Y.T. Zhu, Extraordinary strain hardening by gradient structure, *Proc. Natl. Acad. Sci. USA* 111 (2014) 7197–7201, <http://dx.doi.org/10.1073/pnas.1324069111>.
- [8] X.L. Wu, P. Jiang, L. Chen, J.F. Zhang, F.P. Yuan, Y.T. Zhu, Synergetic strengthening by gradient structure, *Mater. Res. Lett.* 2 (2014) 185–191, <http://dx.doi.org/10.1080/21663831.2014.935821>.
- [9] Y.J. Wei, Y.Q. Li, L.C. Zhu, Y. Liu, X. Lei, G. Wang, Y.X. Wu, Z.L. Mi, J.B. Liu, H.T. Wang, H.J. Gao, Evading the strength–ductility trade-off dilemma in steel through gradient hierarchical nanotwins, *Nature Commun.* 5 (2014) 1–8, <http://dx.doi.org/10.1038/ncomms4580>.
- [10] L.L. Zhu, H.H. Ruan, A.Y. Chen, X. Guo, J. Lu, Microstructures-based constitutive analysis for mechanical properties of gradient-nanostructured 304 stainless steels, *Acta Mater.* 128 (2017) 375–390, <http://dx.doi.org/10.1016/j.actamat.2017.02.035>.
- [11] C.W. Shao, P. Zhang, Y.K. Zhu, Z.J. Zhang, Y.Z. Tian, Z.F. Zhang, Simultaneous improvement of strength and plasticity: Additional work-hardening from gradient microstructure, *Acta Mater.* 145 (2018) 413–428, <http://dx.doi.org/10.1016/j.actamat.2017.12.028>.
- [12] M.X. Yang, Y. Pan, F.P. Yuan, Y.T. Zhu, X.L. Wu, Back stress strengthening and strain hardening in gradient structure, *Mater. Res. Lett.* 4 (2016) 145–151, <http://dx.doi.org/10.1080/21663831.2016.1153004>.
- [13] Y.F. Wang, C.X. Huang, X.T. Fang, H.W. Höppel, M. Göken, Y.T. Zhu, Hetero-deformation induced (HDI) hardening does not increase linearly with strain gradient, *Scr. Mater.* 174 (2020) 19–23, <http://dx.doi.org/10.1016/j.scriptamat.2019.08.022>.
- [14] Z. Cheng, H.F. Zhou, Q.H. Lu, H.J. Gao, L. Lu, Extra strengthening and work hardening in gradient nanotwinned metals, *Science* 362 (2018) eaau1925, <http://dx.doi.org/10.1126/science.aau1925>.
- [15] Y.F. Wang, C.X. Huang, M.S. Wang, Y.S. Li, Y.T. Zhu, Quantifying the synergetic strengthening in gradient material, *Scr. Mater.* 150 (2018) 22–25, <http://dx.doi.org/10.1016/j.scriptamat.2018.02.039>.
- [16] Y.T. Zhu, X.L. Wu, Perspective on hetero-deformation induced (HDI) hardening and back stress, *Mater. Res. Lett.* 7 (2019) 393–398, <http://dx.doi.org/10.1080/21663831.2019.1616331>.
- [17] Y.T. Zhu, X.L. Wu, Ductility and plasticity of nanostructured metals: differences and issues, *Mater. Today Nano.* 2 (2018) 15–20, <http://dx.doi.org/10.1016/j.mtnano.2018.09.004>.
- [18] F.P. Yuan, D.S. Yan, J.D. Sun, L.L. Zhou, Y.T. Zhu, X.L. Wu, Ductility by shear band delocalization in the nano-layer of gradient structure, *Mater. Res. Lett.* 7 (2019) 12–17, <http://dx.doi.org/10.1080/21663831.2018.1546238>.
- [19] Y.F. Wang, C.X. Huang, Q. He, F.J. Guo, M.S. Wang, L.Y. Song, Y.T. Zhu, Heterostructure induced dispersive shear bands in heterostructured Cu, *Scr. Mater.* 170 (2019) 76–80, <http://dx.doi.org/10.1016/j.scriptamat.2019.05.036>.
- [20] C.X. Huang, Y.F. Wang, X.L. Ma, S. Yin, H.W. Höppel, M. Göken, X.L. Wu, H.J. Gao, Y.T. Zhu, Interface affected zone for optimal strength and ductility in heterogeneous laminate, *Mater. Today* 21 (2018) 713–719, <http://dx.doi.org/10.1016/j.mattod.2018.03.006>.
- [21] G. He, J. Eckert, W. Löser, L. Schultz, Novel Ti-base nanostructure–dendrite composite with enhanced plasticity, *Nature Mater.* 2 (2003) 33–37, <http://dx.doi.org/10.1038/nmat792>.
- [22] Y.F. Wang, C.X. Huang, Y.S. Li, F.J. Guo, Q. He, M.S. Wang, X.L. Wu, R.O. Scattergood, Y.T. Zhu, Dense dispersed shear bands in gradient-structured Ni, *Int. J. Plast.* 124 (2020) 186–198, <http://dx.doi.org/10.1016/j.ijplas.2019.08.012>.
- [23] X. Wang, Y.S. Li, Q. Zhang, Y.H. Zhao, Y.T. Zhu, Gradient structured copper by rotationally accelerated shot peening, *J. Mater. Sci. Technol.* 33 (2017) 758–761, <http://dx.doi.org/10.1016/j.jmst.2016.11.006>.
- [24] L. Yang, L. Lu, The influence of sample thickness on the tensile properties of pure Cu with different grain sizes, *Scr. Mater.* 69 (2013) 242–245, <http://dx.doi.org/10.1016/j.scriptamat.2013.04.009>.
- [25] J. An, Y.F. Wang, Q.Y. Wang, W.Q. Cao, C.X. Huang, The effects of reducing specimen thickness on mechanical behavior of cryo-rolled ultrafine-grained copper, *Mater. Sci. Eng. A* 651 (2016) 1–7, <http://dx.doi.org/10.1016/j.msea.2015.10.091>.
- [26] S. Cheng, E. Ma, Y. Wang, L. Kecskes, K. Youssef, C. Koch, U. Trociewitz, K. Han, Tensile properties of in situ consolidated nanocrystalline Cu, *Acta Mater.* 53 (2005) 1521–1533, <http://dx.doi.org/10.1016/j.actamat.2004.12.005>.
- [27] H. Azizi, H.S. Zurob, D. Embury, X. Wang, K. Wang, B. Bose, Using architected materials to control localized shear fracture, *Acta Mater.* 143 (2018) 298–305, <http://dx.doi.org/10.1016/j.actamat.2017.10.027>.
- [28] D. Jia, K.T. Ramesh, E. Ma, Effects of nanocrystalline and ultrafine grain sizes on constitutive behavior and shear bands in iron, *Acta Mater.* 51 (2003) 3495–3509, [http://dx.doi.org/10.1016/S1359-6454\(03\)00169-1](http://dx.doi.org/10.1016/S1359-6454(03)00169-1).
- [29] M. Huang, C. Xu, G.H. Fan, E. Maawad, W.M. Gan, L. Geng, F.X. Lin, G.Z. Tang, H. Wu, Y. Du, D.Y. Li, K.S. Miao, T.T. Zhang, X.S. Yang, Y.P. Xia, G.J. Cao, H.J. Kang, T.M. Wang, T.Q. Xiao, H.L. Xie, Role of layered structure in ductility improvement of layered Ti–Al metal composite, *Acta Mater.* 153 (2018) 235–249, <http://dx.doi.org/10.1016/j.actamat.2018.05.005>.
- [30] Y.F. Wang, M.X. Yang, X.L. Ma, M.S. Wang, K. Yin, A.H. Huang, C.X. Huang, Improved back stress and synergetic strain hardening in coarse-grain/nanostructure laminates, *Mater. Sci. Eng. A* 727 (2018) 113–118, <http://dx.doi.org/10.1016/j.msea.2018.04.107>.
- [31] A. Chen, D. Li, J. Zhang, H. Song, J. Lu, Make nanostructured metal exceptionally tough by introducing non-localized fracture behaviors, *Scr. Mater.* 59 (2008) 579–582, <http://dx.doi.org/10.1016/j.scriptamat.2008.04.048>.
- [32] R.J. Asaro, Micromechanics of crystals and polycrystals, in: *Adv. Appl. Mech.*, Elsevier, 1983, pp. 1–115, [http://dx.doi.org/10.1016/S0065-2156\(08\)70242-4](http://dx.doi.org/10.1016/S0065-2156(08)70242-4).
- [33] X. Sun, K.S. Choi, W.N. Liu, M.A. Khaleel, Predicting failure modes and ductility of dual phase steels using plastic strain localization, *Int. J. Plast.* 25 (2009) 1888–1909, <http://dx.doi.org/10.1016/j.ijplas.2008.12.012>.